Overview:

In this project, experiments and research activities were conducted in collaboration between investigators at the University of Alabama (UA), Georgia Institute of Technology (GT), Lawrence Berkeley National Laboratory (LBNL), Brookhaven National Laboratory (BNL), the DOE Joint Genome Institute (JGI), and the Stanford Synchrotron Radiation Light source (SSRL) to: (i) confirm that phosphatase activities of subsurface bacteria in Area 2 and 3 from the Oak Ridge Field Research Center result in solid U-phosphate precipitation in aerobic and anaerobic conditions; (ii) investigate the eventual competition between uranium biomineralization via U-phosphate precipitation and uranium bioreduction; (iii) determine subsurface microbial community structure changes of Area 2 soils following organophosphate amendments; (iv) obtain the complete genome sequences of the *Rahnella* sp. Y9-602 and the type-strain *Rahnella aquatilis* ATCC 33071 isolated from these soils; (v) determine if polyphosphate accumulation and phytate hydrolysis can be used to promote U(VI) biomineralization in subsurface sediments; (vi) characterize the effect of uranium on phytate hydrolysis by a new microorganism isolated from uranium-contaminated sediments (vii) utilize positron-emission tomography to label and track metabolically-active bacteria in soil columns, and (viii) study the stability of the uranium phosphate mineral product. Microarray analyses and mineral precipitation characterizations were conducted in collaboration with DOE SBR-funded investigators at LBNL.

A full description of the research activities for this award is provided below in items 1-5. UA, in collaboration with LBNL, conducts all of the PhyloChip analyses providing genomic DNA for data analyses (#1). UA conducted all work for JGI sequencing activities including proposal submission to the Community Sequencing Program, licensing forms, and genomic DNA preparation (#2). UA, in collaboration with BNL, conducts all soil column positron emission tomography (PET) studies (#3). GT was the lead on all phytate soil slurry studies described in (#4). UA and GT conducted scheduled meetings via email, conference calls, and/or Skype to plan and design experiments and to assist with troubleshooting, data analyses, and manuscript planning with UA and GT lab personnel. At least two or three times a year, UA and GT lab personnel met at GT, UA, and during the SBR PIs meeting.

Summary of results:

(1). ***Aerobic and Anaerobic U biomineralization study with contaminated ORFRC flow-through columns***. Flow-through columns loaded with ORFRC Area 3 soil were utilized to investigate if (1) indigenous ORFRC soil bacteria exhibited phosphatase activity when provided with an organophosphate substrate under both aerobic and anaerobic conditions and (2) sufficient phosphate was produced to precipitate substantial soluble U(VI). Four flow-through columns containing Area 3 soils were amended continuously with either aerobic or degassed synthetic groundwater (10 mM NO_3^-, 1 mM SO_4^{2-}, 10 mM Ca^{2+}, pH 5.5). Either Glycerol-3-phosphate (G3P) in aerobic conditions (Beazley et al., 2011) or Glycerol-2-phosphate (G2P) in anaerobic conditions (**Figure 1**) was added to all columns once oxygen was removed, but only for two weeks in the U amended control columns. High concentrations of phosphate (1–3 mM) were detected in the effluent of the aerobic columns at both pH compared to aerobic control columns amended with U(VI) only, suggesting that phosphatase-liberating aerobic microorganisms were readily stimulated by the organophosphate substrate. Net phosphate production rates were higher in the low pH soil (0.73 ± 0.17 mM d^{-1}) compared to the circumneutral pH soil (0.43 ± 0.31 mM

d^{-1}), suggesting that non-specific acid phosphatase activity was expressed constitutively in these soils. In anaerobic conditions, nitrate was reduced immediately and completely in the presence of G2P (**Figure 1A**). Sulfate reduction was not significant, likely because of the excess nitrate in the incubations. When G2P was removed from the input solution (U control), nitrate reduction ceased completely. Hydrolysis of G2P produced up to 6 mM of total dissolved phosphate in the columns (**Figure 1B**), suggesting that nitrate-reducing microbial communities hydrolyzed G2P. The pH increased in the anaerobic columns upon G2P amendments, probably because nitrate respiration produced significant amounts of carbonates. Uranium was continuously removed from the effluent in both the U control and G2P amended anaerobic columns, suggesting that it was mainly adsorbed in the absence of G2P (U control column) and precipitated as U(VI) phosphate minerals in the presence of G2P (**Figure 1B**). Nitrate reduction and G2P hydrolysis were persistent even in the presence of U(VI) in the anaerobic conditions. Even though U(VI) was removed in both treatments, the high net production rates of phosphate in the G2P-amended columns suggest that U(VI) biomineralization also occurred in anaerobic conditions. A sequential solid-phase extraction scheme (**Figure 1C**) and X-ray absorption spectroscopy measurements (not shown) were combined to demonstrate that U(VI) was primarily precipitated as uranyl phosphate minerals at low pH, whereas it was mainly adsorbed to iron oxides and partially precipitated as uranyl phosphate at circumneutral pH. Overall, these results demonstrate that the biomineralization of uranium phosphate minerals is a viable bioremediation strategy in both the vadose (i.e. aerobic) and saturated (i.e. anaerobic) zones of aquifers at both low and high pH providing an organophosphate source is available. One manuscript synthesizing these findings was published (Beazley et al., 2011) and another one is in preparation (Williams et al., 2015).

(2). ***Competition between uranium biomineralization via U-phosphate precipitation and uranium bioreduction:*** Although bioreduction of uranyl ions (U(VI)) and biomineralization of U(VI)-phosphate minerals are both able to immobilize uranium in contaminated sediments, the competition between these processes and the role of anaerobic respiration in the biomineralization of U(VI)-phosphate minerals has yet to be investigated. In this study, contaminated sediments incubated anaerobically in static microcosms at pH 5.5 and 7.0 were amended with the organophosphate glycerol-2-phosphate (G2P) as sole phosphorus and external carbon source and iron oxides, sulfate, or nitrate as terminal electron acceptors to determine the most favorable geochemical conditions to these two processes. While sulfate reduction was not observed even in the presence of G2P at both pHs, iron reduction was more significant at circumneutral pH irrespective of the addition of G2P (**Figure 2**). In turn, nitrate reduction was stimulated by G2P at both pH 5.5 and 7.0, suggesting nitrate-reducing bacteria provided the main source of inorganic phosphate in these sediments. U(VI) was rapidly removed from solution in all treatments (**Figure 2I and J**) but was not reduced as determined by X-ray absorption near edge structure (XANES) spectroscopy (not shown). Simultaneously, wet chemical extractions (**Figure 2K and L**) and extended X-ray absorption fine structure (EXAFS) spectroscopy of these sediments (not shown) indicated the presence of U-P species in reactors amended with G2P at both pHs. The rapid removal of dissolved U(VI), the simultaneous production of inorganic phosphate, and the existence of U-P species in the solid phase indicate that uranium was precipitated as U(VI)-phosphate minerals in sediments amended with G2P. Thus, under reducing conditions and in the presence of G2P, bioreduction of U(VI) was outcompeted by the

biomineralization of U(VI)-phosphate minerals and U(VI) sorption at both pHs. These findings were published in a manuscript (Salome et al., 2013).

(3). ***Microbial community structure of subsurface soils amended with glycerol-2-phosphate or glycerol-3-phosphate:*** The phosphatase activity demonstrated by the extant microbial community within Area 2 (FB107-04-00) soil slurries, incubated under oxic conditions at pH 5.5 and with glycerol-2-phosphate (G2P) was detected as early as 96 h following G3P amendments and after 288 h in G2P amendments (**Figure 3A** and **B**). The lack of mass balance between G2P concentration and orthophosphate indicated the potential sequestration of phosphate as polyphosphate granules (**Figure 3C**). Following incubations, total DNA extractions revealed a greater amount of biomass production in G2P treatments (**Figure 3A**). Total archaeal and bacterial richness assessed by the PhyloChip microarray prior to treatments were dominated by *Euryarchaeota, Actinobacteria, Firmicutes,* and *Proteobacteria* communities (**Figures 4A** and **4B**). Following soil slurry treatments, NMDS analysis demonstrated significant changes in community structure (**Figures 4C** and **D**). Archeal and bacterial changes in relative abundance were assessed relative to treatments that were maintained at the same pH but lacked organophosphate amendments (**Figures 5A-D**). Acidic pH treatments enriched a community that was dominated by *Proteobacteria* while pH 6.8 treatments enriched a community that was had nearly equal distribution of OTUs from the phyla *Bacteroidetes* and *Proteobacteria*. Interestingly, Within G2P treatments at either pH, Alphaprotobacteria accounted for greater than 50% of all proteobacterial OTUs. Conversely, the proteobacterial OTUs in G3P treatments at were composed of greater that 95% *Gammaproteobacteria*. This study resulted in one publication (Martinez et al., 2014).

(4). ***DOE JGI sequencing of Rahnella strains:*** The genomes for *Rahnella* sp.Y9602 and *Rahnella aquatilis* CIP 78.65 are complete and publically available on NCBI. We have begun comparative genomic studies to examine the potential influence ORFRC contaminants had on shaping on horizontal gene transfer (HGT) and how these HGT events influence genome architecture (**Figure 6**). Signifcant difference between the two *Rahnella* genomes also include ~280,000 SNPs, ~4,000 small indels, and ~900 rearrangements (**Figure 7**). The average nucleotide identity (ANI) of both genomes is 92.7%, this is significantly lower than the 95% ANI that corresponds to 70% DNA-DNA hybridization of similar species. Currently, we are examining phenotypic differences that will support the description of the *Rahnella* sp.Y9602 as a new species within the genus *Rahnella*. This study resulted in two publications (Martinez et al., 2012a and 2012b).

Additionally, the data from these sequencing projects have supported initiation of biochemical studies of 5 putative acid phosphatase genes from the *Rahnella* sp.Y9602 strain (**Figure 8**) aimed at identifying the contribution of these enzymes to organophosphate hydrolysis under conditions relevant to ORFRC subsurface conditions (e.g. low pH, varying metal and radionuclide concentrations). Preliminary examination of one of the cloned acid phosphatases from *Rahnella* sp. Y9602, most closely related to glucose-1-phosphatase, has yielded variable temperature- and pH-optima based on substrate (**Figure 9**). Further experiments examining acid phosphatase activity will identify the influence of metals and uranium at concentrations relevant to ORFRC subsurface conditions.

(5). ***Phytate as natural organophosphate source to immobilize U(VI) in subsurface sediments***: Contaminated sediments were incubated aerobically in two pH conditions to examine the potential of utilizing phytate, a naturally-occurring and abundant organophosphate in soils, as a phosphorous source to promote U(VI)-phosphate biomineralization by natural microbial communities. Phytate carries a highly negative charge of between -6 and -9 (**Figure 10A**) and, thus, is expected to interact strongly with positively charged uranyl hydroxide complexes at or below circumneutral pH, providing carbonates are not present in significant concentrations. Equilibration of increasing concentrations of phytate with 200 µM dissolved uranium revealed concentration-dependent uranyl solubilities at both pH 5.5 and 7.0 (**Figure 10B**), likely due to the highly negative charge of IP_6 at both pHs (**Figure 10A**). At aqueous [IP_6]:[U] ratios below 15:1, uranium formed precipitates with IP_6 at both pH 5.5 and 7.0 (**Figure 10B**). At or above [IP_6]:[U] ratios of 15:1, however, uranium predominantly remained in solution at both pHs (**Figure 10B**). Previous studies have demonstrated similar concentration-dependent uranyl solubility in the presence of other organophosphates (Beazley et al., 2007), and the increase in uranium solubility with elevated phytate concentration is thought to be caused by enhanced electronic repulsion as the negatively charged phytate concentration increases around the uranium phytate complex. These findings have important implications for promotion of U(VI)-phosphate biomineralization by phytate, as the [IP_6]:[U] ratio likely determines whether chemical (low concentrations of phytate) or biological (high concentrations of phytate) sequestration processes dominates.

Although phytate hydrolysis was not evidenced at pH 7.0, nearly complete hydrolysis was observed both with and without electron donor at pH 5.5 (**Figure 10C**), suggesting indigenous microorganisms express acidic phytases in these sediments. While the rate of hydrolysis of phytate generally increased in the presence of uranium (**Figure 11C** and **D**), the net rate of inorganic phosphate production in solution (**Figure 10C**) was decreased and inositol phosphate intermediates were generated (**Figure 11C** and **D**) in contrast to similar incubations conducted without uranium (**Figure 10C** and **Figure 11A** and **B**). These findings suggest uranium stress increased expression of phytase and simultaneously inhibited phosphatase production and/or activity by the indigenous population that allowed accumulation of inositol phosphate intermediates. Finally, phytate hydrolysis drastically decreased uranium solubility (**Figure 11D**), likely due to formation of ternary sorption complexes, U(VI)-phytate precipitates, and U(VI)-phosphate minerals. Sequential extractions of ORFRC sediments incubated at pH 5.5 and 7.0 in the presence of elevated uranium concentrations reveal a significant shift in solid-phase uranium speciation between slurries with and without phytate (**Figure 12A** and **B**). Without phytate, uranium was primarily associated with Mg^{2+} exchangeable, acetate extractable, and hydroxylamine extractable fractions at both pH 5.5 (**Figure 12A**) and 7.0 (**Figure 12B**), indicating the presence of loosely sorbed uranium species and uranium precipitates (i.e. schoepite). Interestingly, solid-phase uranium speciation shifts towards the more recalcitrant hydroxylamine extractable and peroxide extractable fractions upon introduction of phytate at both pHs (**Figure 12**), indicating phytate addition triggers a change in the dominant uranium removal mechanism even when inorganic phosphate is not produced. XANES analyses confirmed that uranium in the solid phase produced remained oxidized in incubations conducted at both pH (**Figure 12C**), and EXAFS analyses indicated that solid-phase uranium in pH 5.5 reactors was likely associated with phosphate through a combination of ternary $=Fe—IP_6—UO_2^{2+}$ surface complexes, U(VI)-phosphate precipitates, and U(VI)-phytate

precipitates (**Figure 12D** and **E**). In contrast, EXAFS analyses of the pH 7.0 incubations displayed no evidence of U(VI)-phosphate, nor U(VI)-phytate precipitates, despite the apparent presence of U(VI)-phytate precipitates in phytate-amended reactors (**Figure 12B**), indicating these precipitates may not represent the dominant form of solid U at this pH. Likely, both uranium sorption to ORFRC sediments and precipitation of U(VI)-IP_6 solid phases contributed to uranium removal in pH 7.0 incubations. Overall, the results of this study provide evidence for the ability of natural microbial communities to liberate phosphate from phytate, possibly as detoxification mechanism, in acidic sediments and demonstrate the potential utility of phytate-promoted uranium immobilization in subsurface environments. This study resulted in the submission of one manuscript, presently in revisions (Taillefert et al., 2015).

(6) Effect of uranium on phytate hydrolysis by a new microorganism isolated from uranium-contaminated sediments: Two phytase-positive microorganisms were isolated from contaminated sediments incubated aerobically in soil slurries (**Figure 13A-E**), and PCR amplified 16S rRNA sequences revealed these isolates as *Bradyrhizobium* and *Variovorax* species. These organisms grow aerobically on lactate, acetate, and formate (**Figure 13F**) and liberate large concentrations of phosphate compared to other known phosphatase-hydrolyzing or metal-reducing microorganisms (**Figure 13G**). To determine the effect of uranium on phytate hydrolysis by these metal-resistant microorganisms, *Variovorax* sp. was incubated aerobically in pH 5.5 artificial groundwater amended with 1 mM phytate as the sole phosphorus source, 3 mM lactate as the electron donor, and increasing concentrations of uranium (**Figure 13H**). As phytate may chemically precipitate with uranium, live cells were equilibrated with uranium and lactate prior to phytate addition to ensure exposure of *Variovorax* sp. to elevated uranium levels. Lactate consumption was rapid, complete, and accompanied by biomass accumulation in all experimental conditions (not shown), even after a 4 hour equilibration with elevated uranium concentrations. Without uranium, 6 mM inorganic phosphate was liberated by *Variovorax* sp. and almost complete degradation of the initial 1 mM amended phytate was observed after only 2 weeks of incubation (**Figure 13H**). In the presence of uranium, however, total inorganic phosphate production over the two week incubation period decreased linearly with increasing uranium concentrations (not shown), though pseudo-first order rate constants of phytate hydrolysis increased significantly up to 1 mM uranium (**Figure 13H**). In addition, introduction of uranium resulted in earlier onset and more rapid accumulation of inorganic phosphate as well as incomplete degradation of phytate compared to identical reactors without uranium. These findings suggest the existence of a significant uranium toxicity effect to *Variovorax* sp. at low concentrations that is compensated by expressing phytate-hydrolyzing enzymes to immobilize uranium as U(VI)-phosphate minerals. Overall, the results of this study suggest that bacterial phytate hydrolysis may be enhanced in contaminated environments if microorganisms initiate phytase enzyme expression as a uranium detoxification mechanism.

(7). ***PET-imaging of ORFRC Y9602 in soil columns***.

Our recent collaboration with researchers (David Schlyer and Joanna Fowler) at Brookhaven National Laboratory examined the use of positron emission tomography as a tool that will allow metabolically active microooorganisms to be imaged in soil column studies **(Figure 14)**. The ORFRC *Rahnella* sp.Y9602 strain was used as a model microbe for studies that labeled metabolically active cells with 2-deoxy-2-[^{18}F] fluoro-D-glucose (^{18}FDG). Preliminary studies published in the Journal of Hazardous Materials demonstrated the viability of utilizing positron

emitting isotopes for subsurface monitoring of metabolically bacteria. This study resulted in one publication (Kinsella et al., 2012).

(8) Stability of the uranium phosphate mineral product: For U(VI)-phosphate biomineralization via microbially-mediated phytate hydrolysis to be an effective remediation strategy, the U(VI)-phosphate mineral product must remain stable over a broad range of chemical conditions and phytate must remain bioavailable to subsurface microorganisms. In this study, the stability of U(VI)-phosphate minerals exposed to varying pH and varying dissolved inorganic carbon (DIC) and orthophosphate concentrations in artificial groundwater was examined **(Figure 15)**. In low pH conditions representative of the Oak Ridge Field Research Center (ORFRC), U(VI)-phosphate minerals remain stable for at least 6 months, even in the presence of 20 mM DIC (**Figure 15A**). At higher pH, however, U(VI)-phosphate minerals were partially (< 60%) destabilized after 12 days (**Figure 15B**), indicating that U(VI)-phosphate biomineralization is an appropriate remediation strategy for low pH (< 7) or low DIC (< 10 mM) environments. Finally, the effect of polyphosphate compounds on U-P dissolution was not as drastic as observed with carbonates (**Figure 15B** and **C**). Less than 20% U(VI) dissolution was observed in the presence of sodium metaphosphate at pH 7.0, while minimal dissolution occurred in the presence of sodium phytate. Interestingly, uranium dissolution in the presence of these polyphosphate and organophosphate compounds exhibited a positive correlation with the concentration of inorganic phosphate produced in solution (**Figure 15B**). The production of inorganic phosphate in this system far exceeded concentrations expected solely from autunite dissolution (i.e. 200 µM), indicating polyphosphates and/or organophosphates were hydrolyzed. Although the most significant autunite dissolution occurred in metaphosphate-amended systems, uranium minerals dissolved only when phosphate was produced in excess of 3 mM (**Figure 15B**), presumably due to chemical hydrolysis of metaphosphate at pH 4.5, 5.5 and 7.0. At pH 8.0, however, when less than 1 mM orthophosphate accumulated and pH had no effect on autunite stability, metaphosphate did not promote autunite dissolution, suggesting this process was promoted by orthophosphates rather than the polyphosphate source. Thus, the small dissolution of autunite observed at low pH for triphosphate and pH < 8 for meta-phosphate was likely promoted by dissolved inorganic phosphate that accumulated in solution. Overall, these findings suggest that biomineralization strategies utilizing phytate as an organophosphate source will not compromise the stability of the mineral product. These findings were included in a review paper that is presently in press (Belli and Taillefert, 2015).

(9). ***Alabama Launchpad Business Plan Competition***.

We are in the process of translating our findings for phosphorus-mediated bioremediation of uranium and heavy metals to support innovative sustainable agricultural practices. Strains closely related to our phosphorus solubilizing isolates demonstrate antagonistic properties toward common fungal plant pathogens. Such technology transfer of bioremediation-related technology to precision agriculture will allow farmers to more efficiently make use of phosphate present within fertilizers and sequestered within the soils. In an effort to secure funding to develop a microbial based product for agriculture, we entered the 2011-2012 Alabama Launchpad Business Plan Competition and won $30,000 in prize money that will be used to generate additional data for SBIR applications. Participation in the business plan competition has supported collaboration between the Sobecky laboratory and Agricen Sciences to develop methodologies for enrichment of phosphate-solubilizing bacteria important for agricultural applications.

Publications:

(1) Beazley, M.J., Martinez, R.J., Webb, S.M., Sobecky, P.A., and Taillefert, M., 2011. The effect of pH and natural microbial phosphatase activity on the speciation of uranium in subsurface environments. *Geochimica et Cosmochimica Acta* 75: 5648-5663.

(2) Kinsella, K., Schlyer, D.J., Fowler, J.S., Martinez, R.J., and Sobecky, P.A. 2012. Evaluation of positron emission tomography as a method to visualize subsurface microbial processes. *Journal of Hazardous Materials* 213-214:498-501.

(3) Martinez, R. J., Bruce, D., Detter, C., Goodwin, L. A., Han, J., Han, C. S., Held, B., Land, M. L., Mikhailova, N., Nolan, M., Pennacchio, L., Pitluck, S., Tapia, R., Woyke, T., and Sobecky, P. A. 2012a. Complete genome sequence of *Rahnella* sp. Y9602, a Gammaproteobacteria isolate from metal and radionuclide contaminated soil. *Journal of Bacteriology* 194: 2113-2114.

(4) Martinez, R. J., Bruce, D., Detter, C., Goodwin, L. A., Han, J., Han, C. S., Held, B., Land, M. L., Mikhailova, N., Nolan, M., Pennacchio, L., Pitluck, S., Tapia, R., Woyke, T., and Sobecky, P. A. 2012b. Complete genome sequence of *Rahnella aquatilis* CIP 78.65. *Journal of Bacteriology* 194:3020-3021.

(5) Salome, K.R., Green, S.J., Beazley, M.J., Webb, S.M., Kostka, J.E., Taillefert, M., 2013. The role of anaerobic respiration in the immobilization of uranium through biomineralization of phosphate minerals. *Geochimica et Cosmochimica Acta* 106: 344-363.

(6) Martinez, R.J., Wu, C., Beazley, M.J., Andersen, G.L., Conrad, M.E., Hazen, T.C., Taillefert, M., and Sobecky, P.A. 2014. Microbial community responses to organophosphate substrates additions in contaminated subsurface soils. *PLoS ONE* 9(6): e100383.

(7) Martinez, R.J., Beazley, M.J., and Sobecky, P.A. 2014. Phosphate-mediated remediation of metals and radionuclides. *Advances in Ecology* Vol. 2014: 786929.

(8) Belli, K.; Taillefert, M. 2015. Biogeochemical processes regulating the mobility of uranium in contaminated sediments. In: '*Trace elements in waterlogged soils and sediments*' (Jörg Rinklebe; Anna S. Knox; Michael Paller, Eds.). Chapter 7. In press.

(9) Salome, K. R.; Beazley, M. J., Webb, S. M.; Sobecky, P. A.; Taillefert, M. 2015. Uranium biomineralization promoted by microbially-mediated phytate hydrolysis in subsurface soils. In review.

(10) Williams, A., Taillefert, M. 2015. Non-reductive biomineralization of uranium phosphate minerals under anaerobic conditions. In preparation.

Abstracts to National and International Meetings (from UA and GT)

(1) Martinez, R.J., Beazley, M.J., Wu, C., Hazen, T.C., Andersen, G.L., Webb, S.M., Taillefert, M., Sobecky, P.A. 2011. Uranium Biomineralization by Natural Microbial Phosphatase Activities in the Subsurface. U.S. DOE SBR Annual PI Workshop. Washington, DC.

(2) Beazley, M.J., Martinez, R.J., Webb, S.M., Sobecky, P.A., and Taillefert, M., 2011. The effect of pH and natural microbial phosphatase activity on the speciation of uranium in subsurface environments. American Society for Microbiology National Meeting, New Orleans, LA.

(3) Martinez, R.J., Beazley, M.J., Wu, C., Hazen, T.C., Andersen, G.L., Webb, S.M., Taillefert, M., Sobecky, P.A. 2011. Uranium Biomineralization by Natural Microbial Phosphatase Activities in the Subsurface. American Society for Microbiology National Meeting, New Orleans, LA.

(4) Martinez, R.J., Wu, C., Beazley, M.J., Andersen, G.L., Hazen, T.C., Taillefert, M., Sobecky, P.A.. 2011. Uranium Biomineralization by Natural Microbial Phosphatase Activities in the Subsurface. International Society for Subsurface Microbiology. Garmisch-Partenkirchen, Germany.

(5) Martinez, R.J., Wu, C., Beazley, M.J., Andersen, G.L., Hazen, T.C., Taillefert, M., Sobecky, P.A.. 2011. Uranium Biomineralization by Natural Microbial Phosphatase Activities in the Subsurface. American Geophysical Union. San Francisco, CA.

(6) Salome, K.R., Beazley, M.J., Sobecky, P.A., DiChristina, T.J., Taillefert, M. 2011. Potential for utilizing naturally occuring phytate in U(VI) bioremediation strategies. 222nd ACS Meeting, Denver, CO.

(7) A. Williams, K. R. Salome, M. Taillefert. 2011. Assessing the potential for non-reductive biomineralization of uranium by bacterial phosphatase activity in anaerobic environments. 222nd ACS Meeting, Denver, CO.

(8) Sobecky, P.A., Taillefert, M., Martinez, R.J., Wu, C., Salome, K.R., Beazley, M.J., Andersen, G.L., Hazen, T.C., Kinsella, K., Schlyer, D.J., and Fowler, J. 2012. Uranium Biomineralization by Natural Microbial Phosphatase Activities in the Subsurface. U.S. DOE SBR Annual PI Workshop. Washington, DC.

(9) K. R. Salome, M. J. Beazley, R. J. Martinez, P. A. Sobecky, E. J. Tomaszewski, T. J. DiChristina, M. Taillefert. 2012. Effects of Soil Sorption on Organophosphate Bioavailability: Implications for U(VI) Bioremediation Strategies. 244th ACS National Meeting, Philadelphia, PA.

(10) Sobecky, P.A., Taillefert, M., Salome, K.R., Beazley, M.J., Webb S., Martinez, R.J. 2013. A Uranium biomineralization by natural microbial phosphatase activities in the subsurface. 2013 U.S. DOE SBR Annual PI Workshop. Potomac, MD.

Invited Seminars or Contributions (from UA or GT only)

(1) Martinez, R.J. 2010. Microbial Phosphatase Activity Involved in Subsurface Uranium Sequestration. 2010 Summer School in Nuclear and Radiochemistry Lecture Series. Brookhaven National Laboratory, Upton, NY. (invited)

(2) Sobecky, P.A. 2010. Microbial Phosphorus Metabolism: Applications for the Remediation of Metals and Radionuclides (invited seminar, American Society for Microbiology Meeting (Southeastern Branch Meeting), Montgomery AL. (invited)

(3) Taillefert, M., Beazley, M. J., Webb, S., Martinez, R. J., Sobecky, P. A. 2010. Combining X-ray Absorption Spectroscopy with Wet Chemical Techniques to Evaluate the Effect of Natural Phosphatases on the Precipitation of U(VI) Phosphate Minerals in Soils. ACS National Meeting, San Francisco, CA. (invited)

(4) Sobecky, P.A. 2011. Environmental Challenges Mitigated by Microorganisms: from Contaminated Terrestrial Subsurfaces to the Deepwater Horizon Marine Oil Spill, University of Alabama-Birmingham (UAB), Department of Biology (invited)

(5) Sobecky, P.A. 2011. Environmental Challenges Being Met Through Graduate Education; (invited speaker/panel participant; Conference of Southern Graduate Schools; Plenary Session VII: New Pathways to Creative Solutions). Huntsville, AL. (invited)

(6) Taillefert, M. 2012. Biomineralization of U(VI) as bioremediation strategy: Insights from speciation and kinetic studies. Uranium Biogeochemistry Workshop, Monte Verita, Ascona, Switzerland.

(7) Sobecky, P.A. 2014. Natural Attenuation Promoted by Microbial Phosphorus Cycling. Contaminated Site Management: Remediation & Management of Soil, Sediment and Water International Conference (CSM-2014); San Diego, CA. (invited)

(8) Sobecky, P.A. 2014. Microbial Ecosystem Services: Contributions to Restoring Soil and Water Quality. Department of Microbiology, University of Georgia, Athens, GA. (invited)

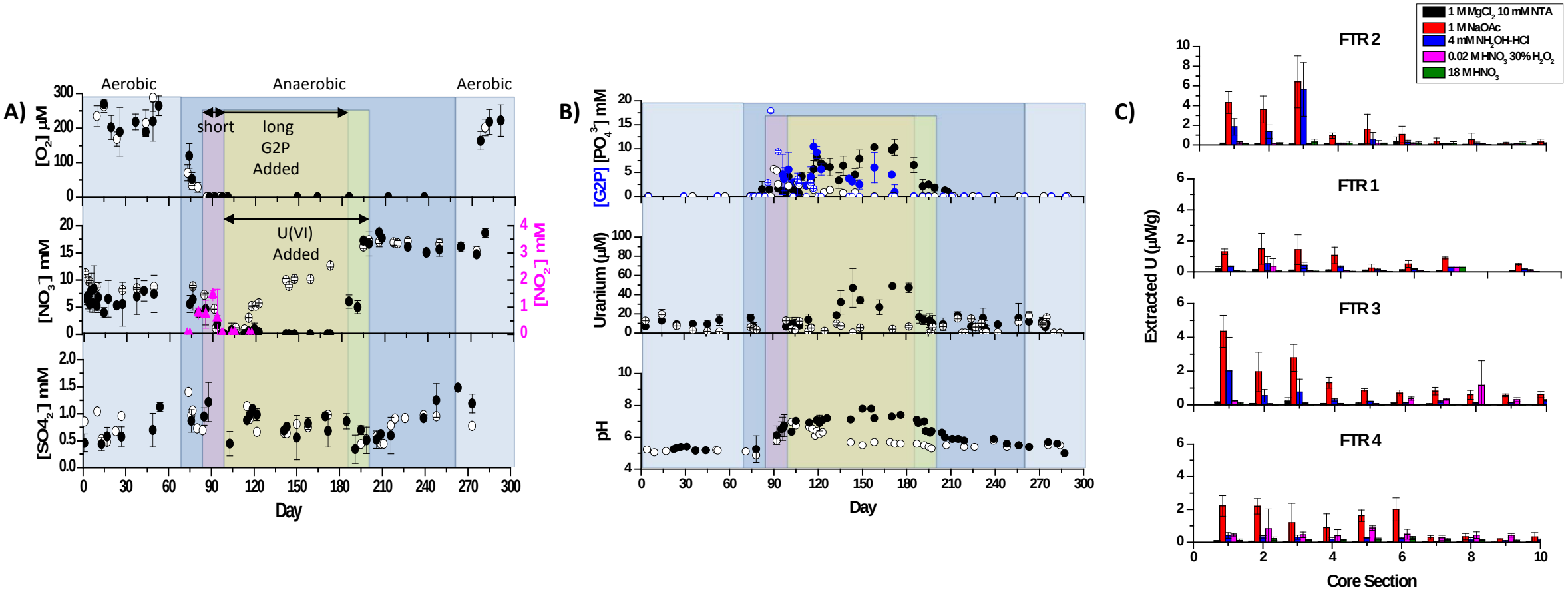

Figure 1. Average concentrations of: (A) dissolved oxygen, nitrate, nitrite, and sulfate, as well as (B) G2P, total soluble phosphate, uranium, and pH measured in the effluent of three flow-through reactors amended with G2P for long times (days 80-190, closed symbols) and one reactor amended with G2P for short times (days 80-96, open symbols). Error bars on symbols refer to the standard deviation of triplicate reactors. (C) Total uranium recovered from Tessier's sequential extraction scheme performed on soils from the short (FTR 2) and long term G2P amended (FTR 1,3,4) reactors after incubation with G2P and 200 µM uranyl acetate. Error bars represent the results of triplicate samples. Note larger scale on FTR 2 graph.

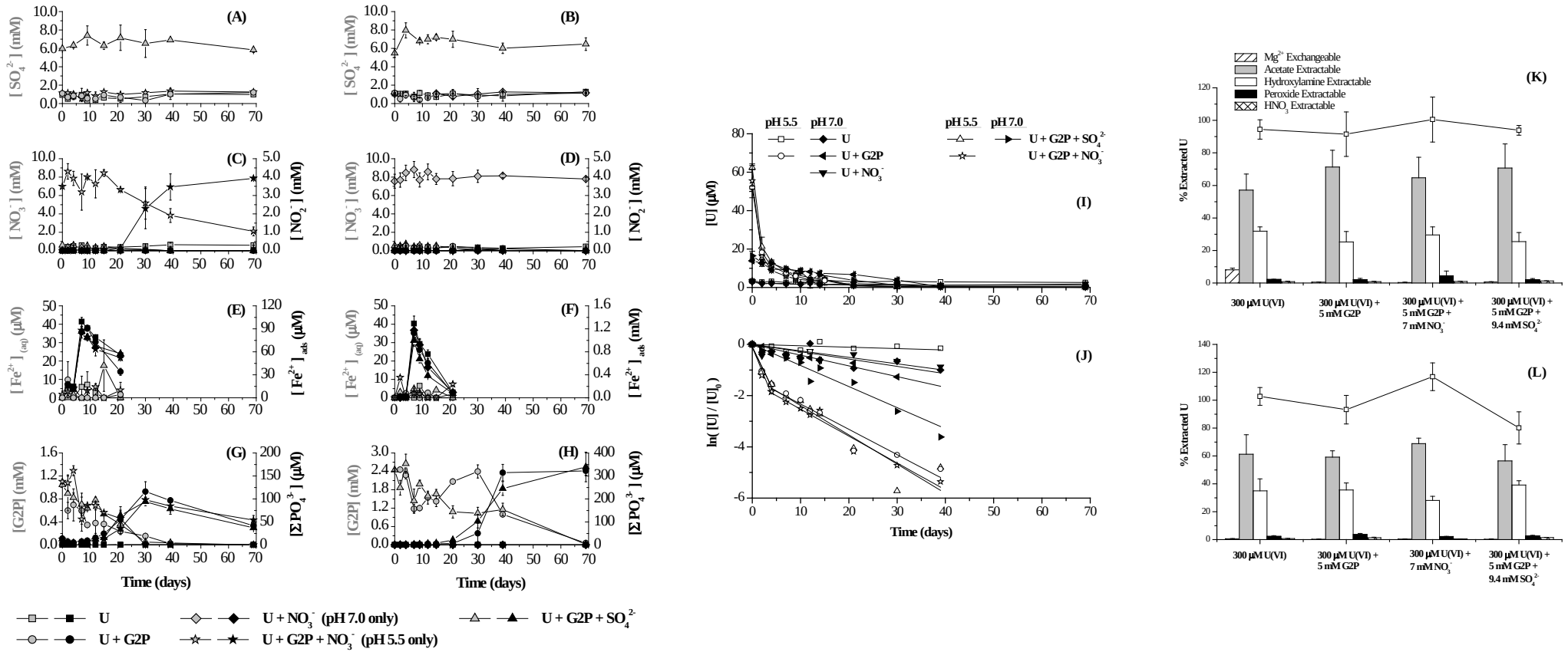

Figure 2. Evolution of SO_4^{2-} [(A) and (B)], NO_3^- and NO_2^- [(C) and (D)], $Fe^{2+}_{(aq)}$ and adsorbed Fe^{2+} [(E) and (F)], and Glycerol-2-phosphate (G2P) and $\sum PO_4^{3-}$ [(G) and (H)] and total dissolved uranium [(I) and (J)] as a function of time in pH 5.5 [(A), (C), (E), (G), (I), and (J)] and pH 7.0 [(B), (D), (F), (H), (I), and (J)] static microcosms amended with 300 µM UO_2^{2+} only; 300 µM UO_2^{2+} and 7 mM NO_3^- (pH 7.0 only); 300 µM UO_2^{2+} and 5 mM G2P; 300 µM UO_2^{2+}, 5 mM G2P, and 7 mM NO_3^- (pH 5.5 only); or 300 µM UO_2^{2+}, 5 mM G2P, and 9.4 mM SO_4^{2-}. Grey symbols represent chemical species on the left axes, while black symbols represent chemical species on the right axes. Error bars represent the range of average reported concentrations between duplicate reactors. Solid phase-associated U extracted by the sequential extraction technique of Tessier (1979) from (K) pH5.5 and (L) pH 7.0 sediments after 70 days of incubation. Bars represent percent uranium extracted in each individual extraction step with respect to the total extracted uranium in each treatment. Symbols represent the percent uranium recovered in each reactor with respect to the total mass of extractable uranium. All error bars represent the standard error of the mean calculated from duplicate reactors and duplicate extractions

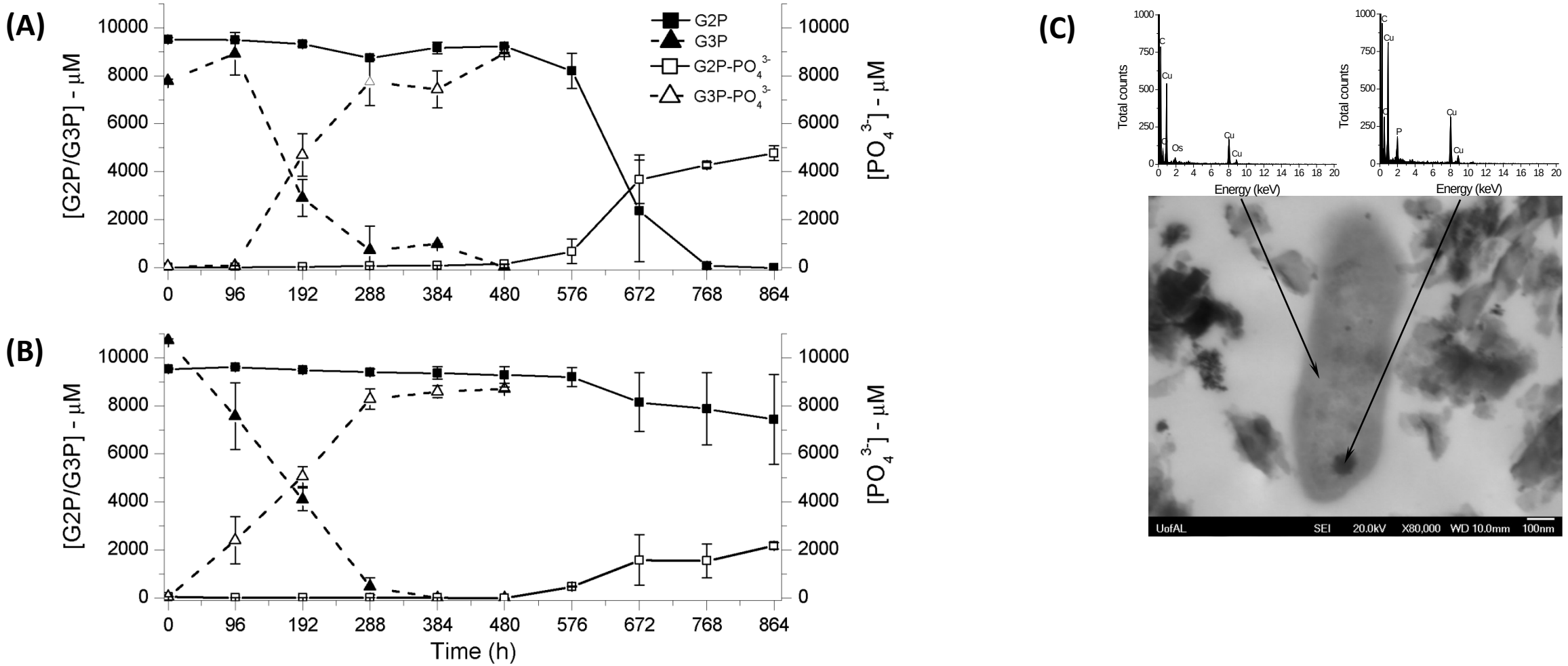

Figure 3. Organophosphate and phosphate measurements. Sediment slurry incubations conducted at (A) pH 5.5 and (B) pH 6.8. Solid lines connect time points in G2P treatments and dashed lines connect time points in G3P treatments. (C) Electron micrographs with EDS analysis of electron dense cytoplasmic structures reveal phosphate rich granules.

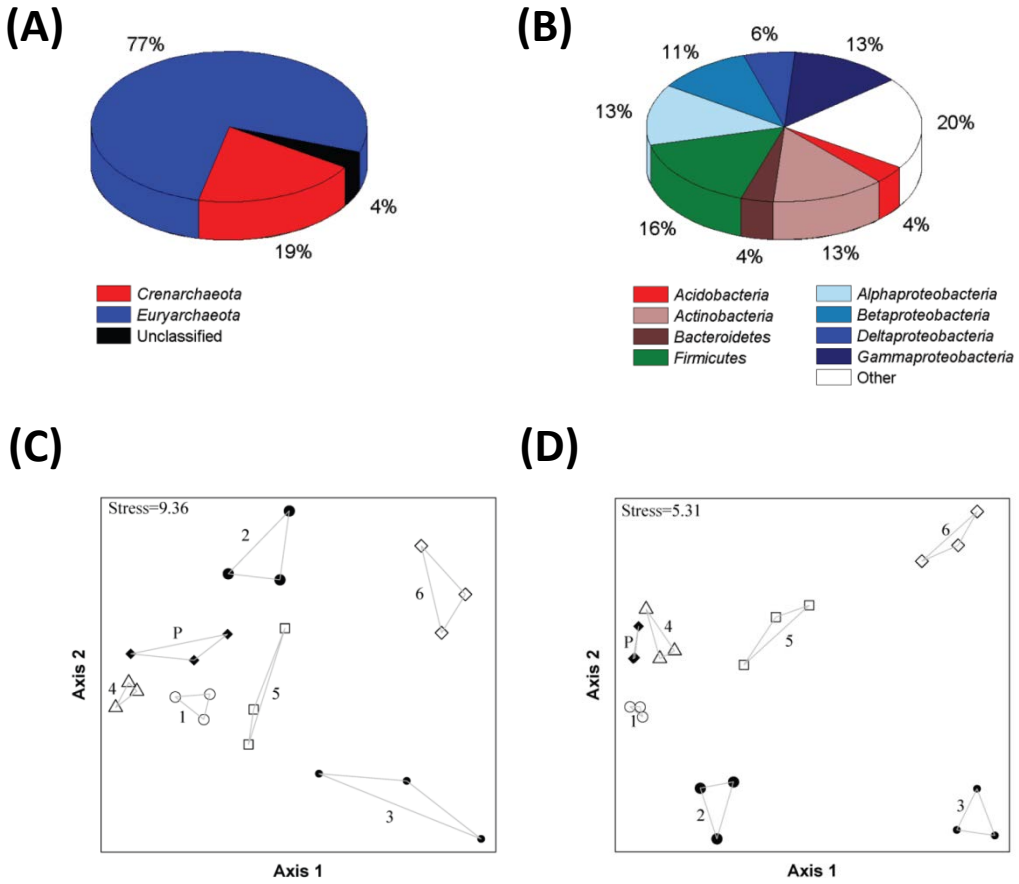

Figure 4. Archaeal and bacterial community structure. Phylum-level richness of (A) *Archaea* and (B) *Bacteria* detected in sediments prior to treatments. (C) NMDS ordination of (C) archaeal and (D) bacterial community distances present within replicate samples. (D) Phylum-level richness of Bacteria detected in sediments prior to treatments. Designations for all samples are as follows: P-sediments prior to treatment, 1-pH 5.5 without organophosphate amendment, 2-pH 5.5 amended with G2P, 3-pH 5.5 amended with G3P, 4-pH 6.8 without organophosphate amendment, 5-pH 6.8 amended with G2P, and 6-pH 6.8 amended with G3P. Phylum-level richness of *Archaea* and *Bacteria* prior to treatments represents the summation of total richness detected from replicate sediment DNA extractions.

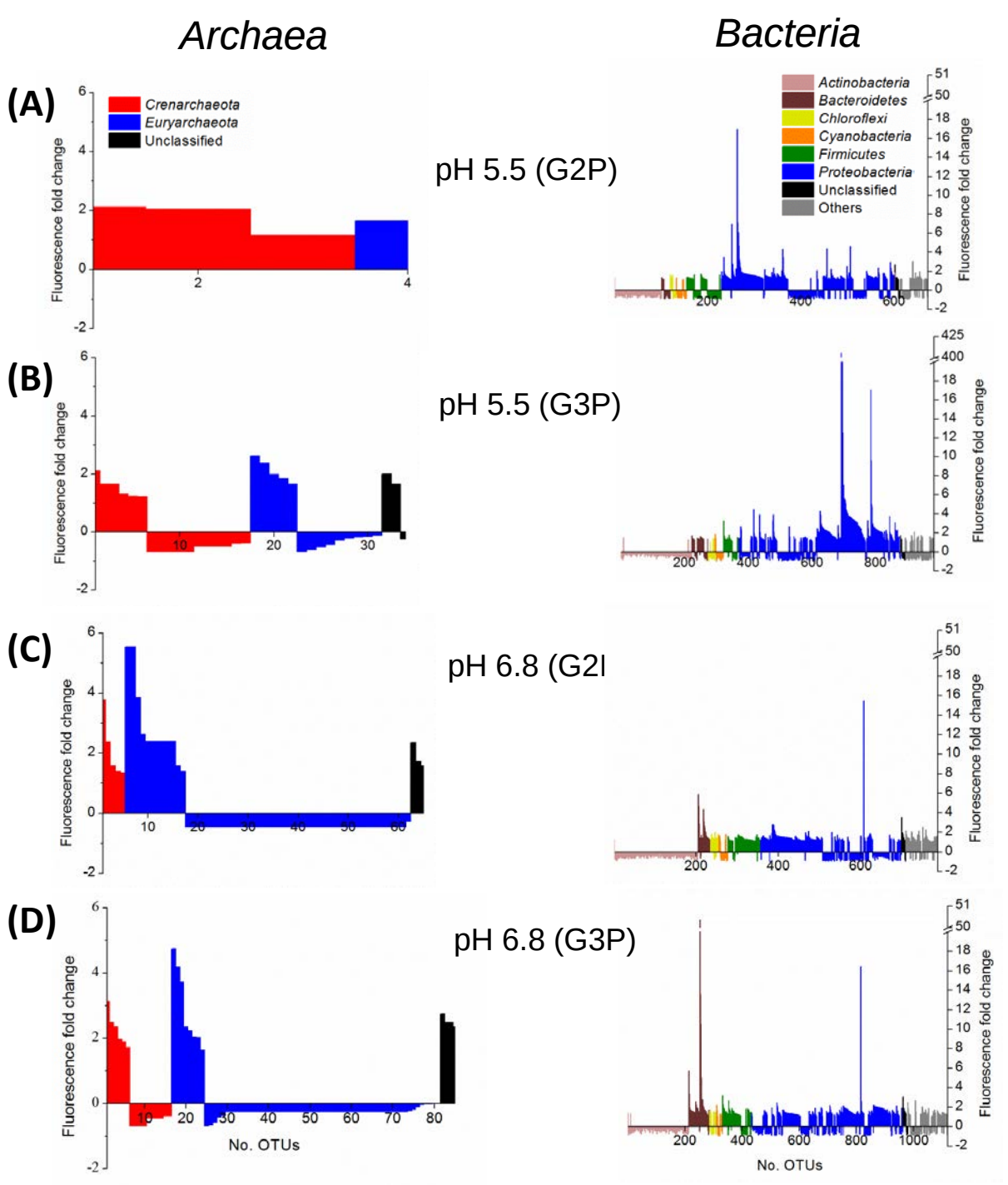

Figure 5. Dynamic archaeal and bacterial OTUs within sediment slurry treatments. Total detected archaeal (left column) and bacterial (right column) OTUs compiled from replicate treatments that significantly increased or decreased relative to incubations lacking organophosphate. Treatment conditions and total number of taxa plotted: (A) G2P (pH 5.5), (B) G3P (pH 5.5), (C) G2P (pH 6.8), and (D) G3P (pH 6.8). OTUs with a 2-fold or greater decrease in fluorescence were not detected.

Rahnella aquatilis ATCC 33071

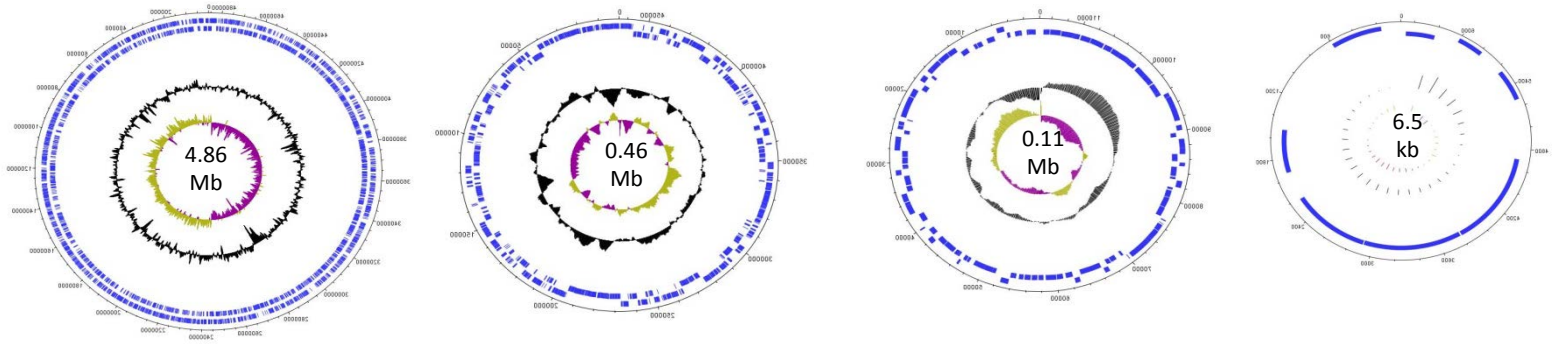

Rahnella sp. Y9602

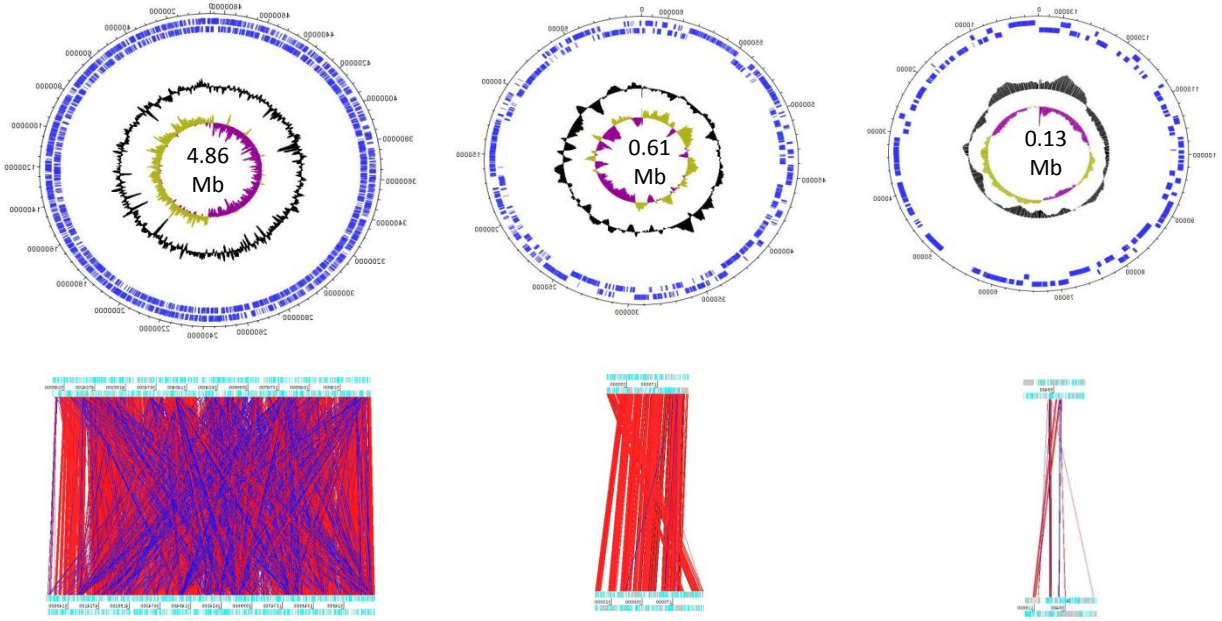

Figure 6. Chromosome and plasmid maps of *Rahnella aquatilis* (ATCC 33071) and *Rahnella* sp. Y9602. Sequence alignments of chromosomes and plasmids of similar size are presented below each nucleic acid element.

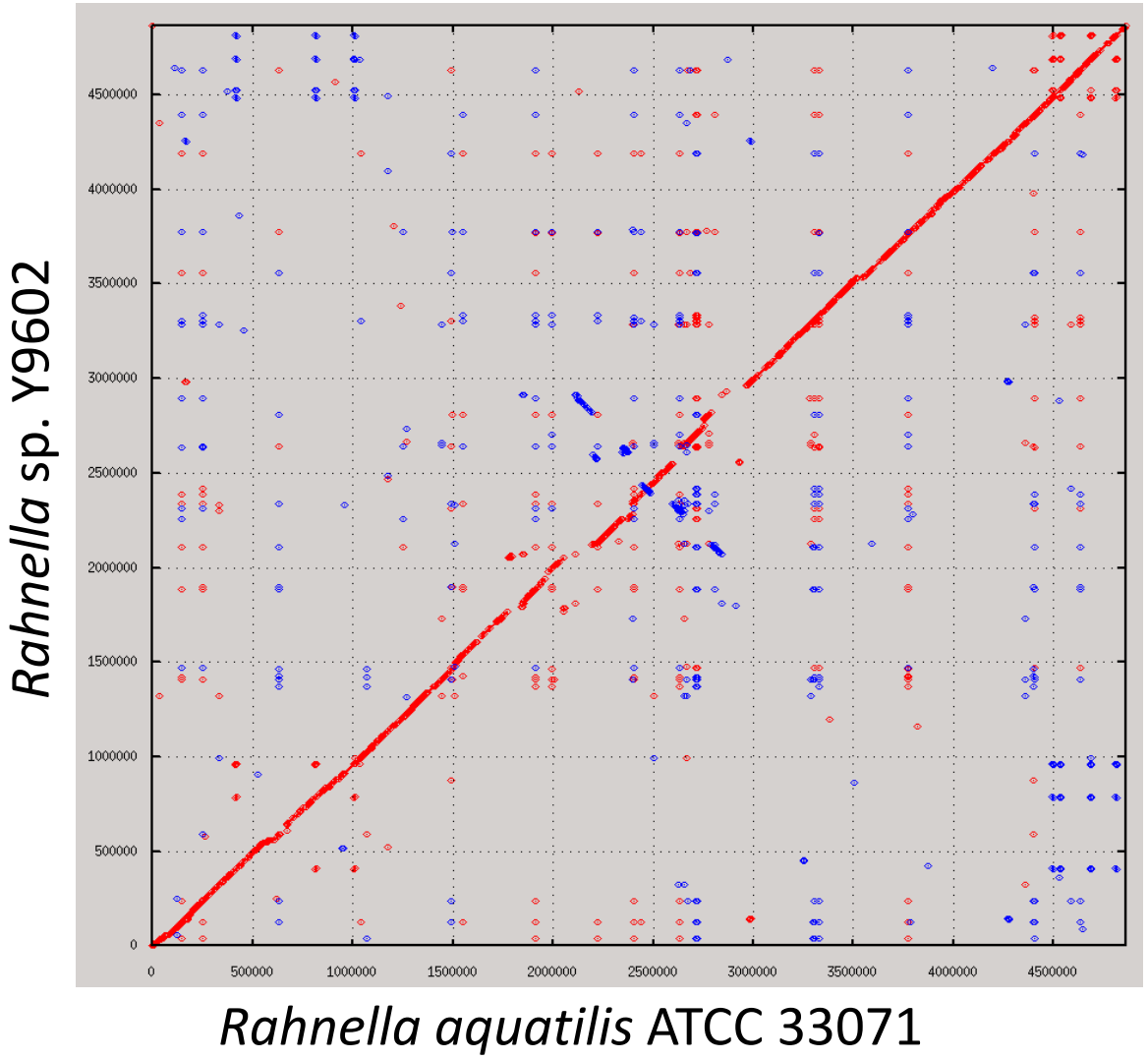

Figure 7. Alignment of *Rahnella* aquatilis ATCC 33071 and *Rahnella* sp. Y9602 chromosomes. The average nucleotide identity between both genomes was calculated to be 92.7%

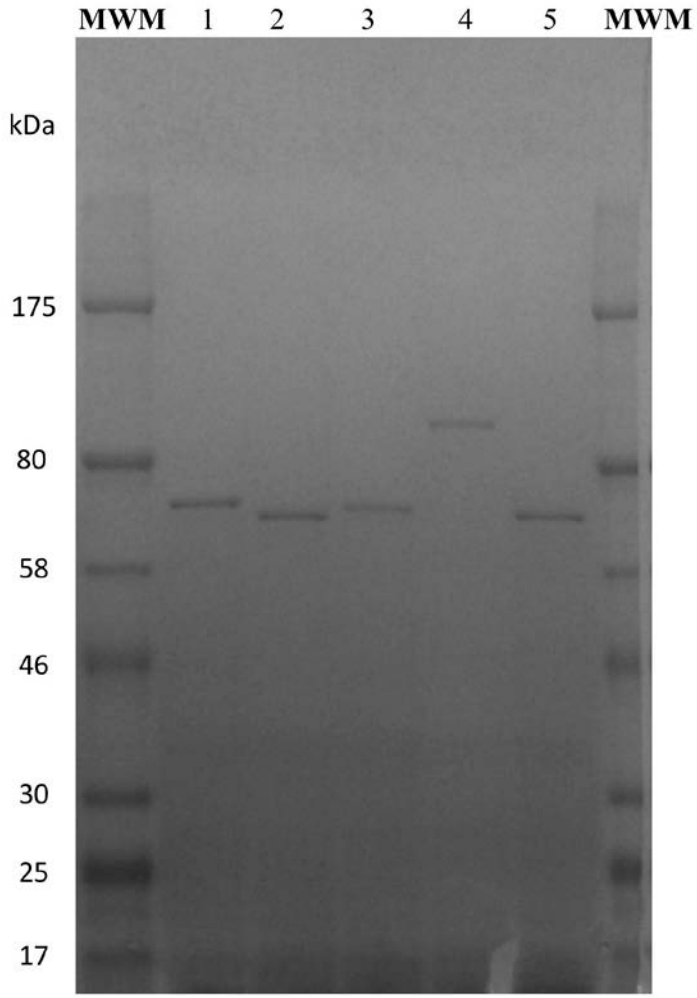

Figure 8. Coomassie staining of five low-molecular weight acid phosphatases encoded by ORFRC *Rahnella* sp. Y9602.

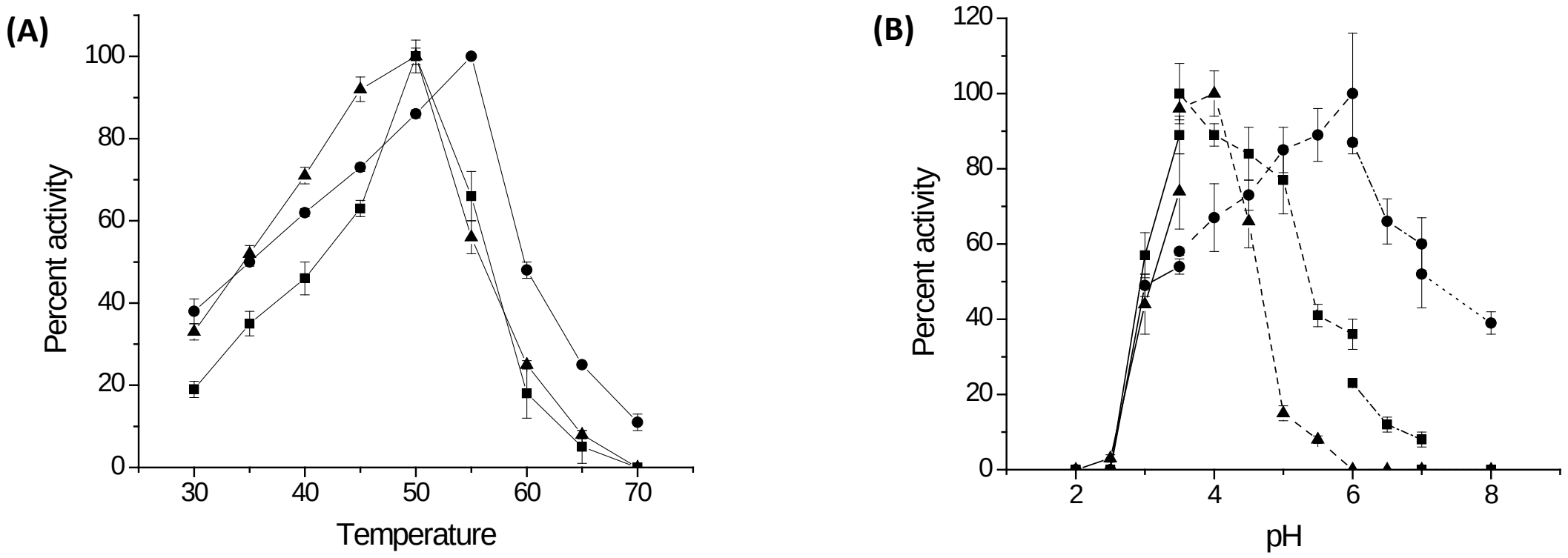

Figure 9. Biochemistry of *Rahnella* sp. Y9602 glucose-1-phosphatase. (A) Temperature-dependent activity of *Rahnella* sp. Y9602 glucose-1-phosphatase. Solid lines connect temperature treatments with 10 mM paranitrophenol phosphate (■), 5 mM glucose-1-phosphate (●), and 5mM inositol-6-phosphate (▲). All incubations were incubated in 100 mM sodium acetate (pH 6) for 5 min. Reaction was terminated with addition of 0.2 M sodium hydroxide (0.8 ml).(B) pH-dependent activity of *Rahnella* sp. Y9602 glucose-1-phosphatase. Substrates utilized included: 10 mM paranitrophenol phosphate (■), 5 mM glucose-1-phosphate (●), and 5mM inositol-6-phosphate (▲). All incubations were utilized the following buffers at a final concentration of 100 mM for 5 min. Buffers Glycine/HCl (—) from pH 2.0-3.5, Sodium acetate (- - -) from pH 3.5-6.0, Tris/Acetic acid (-·-), and Tris/HCl (-----) from pH 7.0-8.0. Reaction was terminated with addition of 0.2 M sodium hydroxide (0.8 ml).

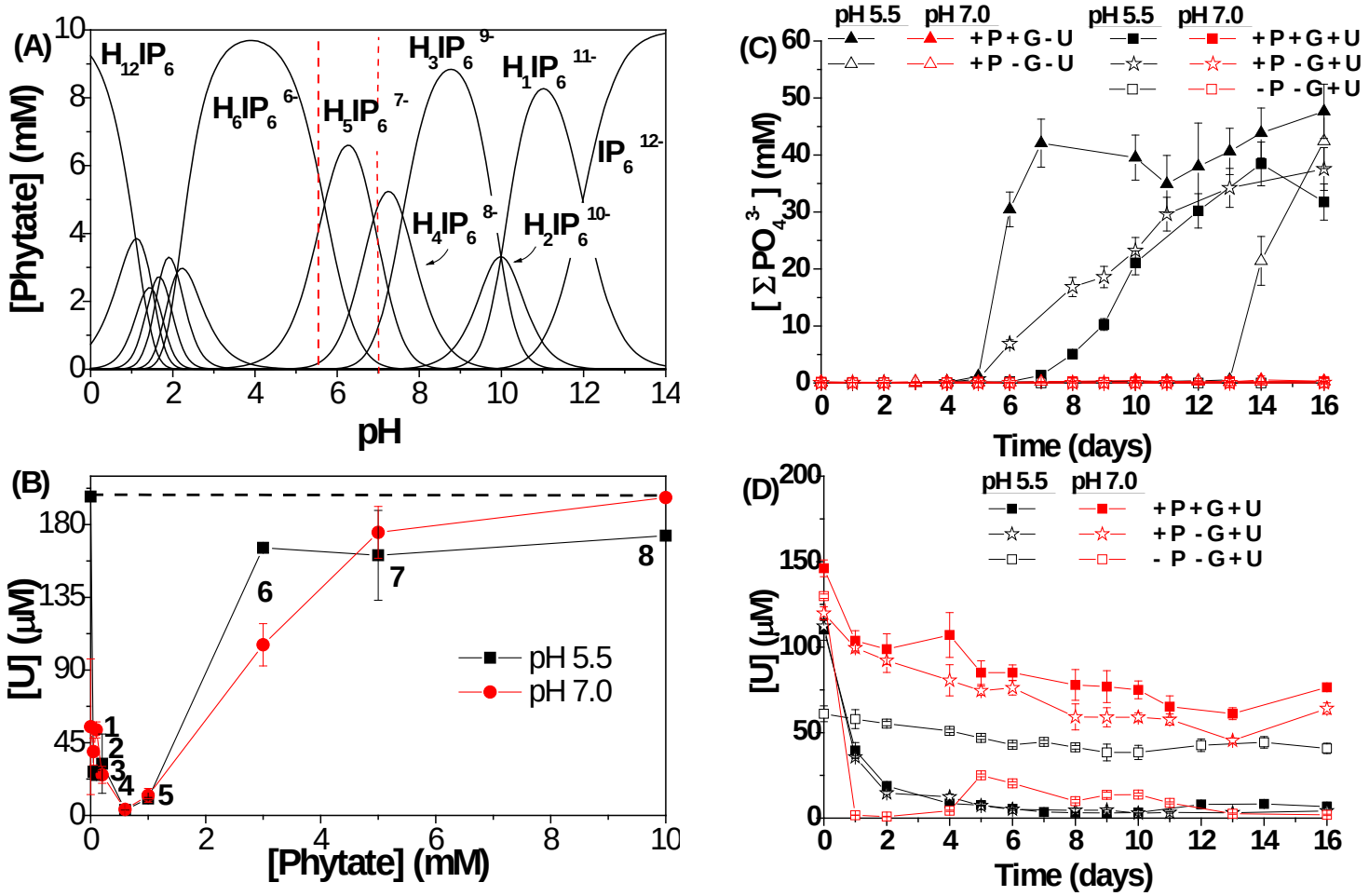

Figure 10. (A) Calculated phytate (IP_6) speciation as a function of pH. Vertical dashed lines represent the experimental conditions of the present study. (B) Solubility of 200 µM uranium (dashed line) in the presence of increasing concentrations of phytate at both pH 5.5 (black squares) and 7.0 (red circles) in artificial groundwater. Labels 1, 2, 3, 4, 5, 6, 7, and 8 represent [IP_6]:[U] molar ratios of 1:4, 1:2, 1:1, 3:1, 5:1, 15:1, 25:1 and 50:1. (C) Evolution of inorganic phosphate (ΣPO_4^{3-}) and (D) dissolved uranium as a function of time in pH 5.5 (black) and pH 7.0 (red) soil slurries containing 16 g/L Area 3 Oak Ridge Field Research Center soils and artificial groundwater amended with 10 mM phytate and 10 mM glycerol (+ P + G – U); 10 mM phytate only (+ P - G – U); 10 mM phytate, 10 mM glycerol, and 200 µM UO_2^{2+} (+ P + G + U); 10 mM phytate and 200 µM UO_2^{2+} (+ P - G + U) and 200 µM UO_2^{2+} only (- P - G + U). Closed symbols represent slurries amended with glycerol and triangles represent slurries without uranium. Error bars include variation between triplicate reactors and the analytical error on duplicate measurements

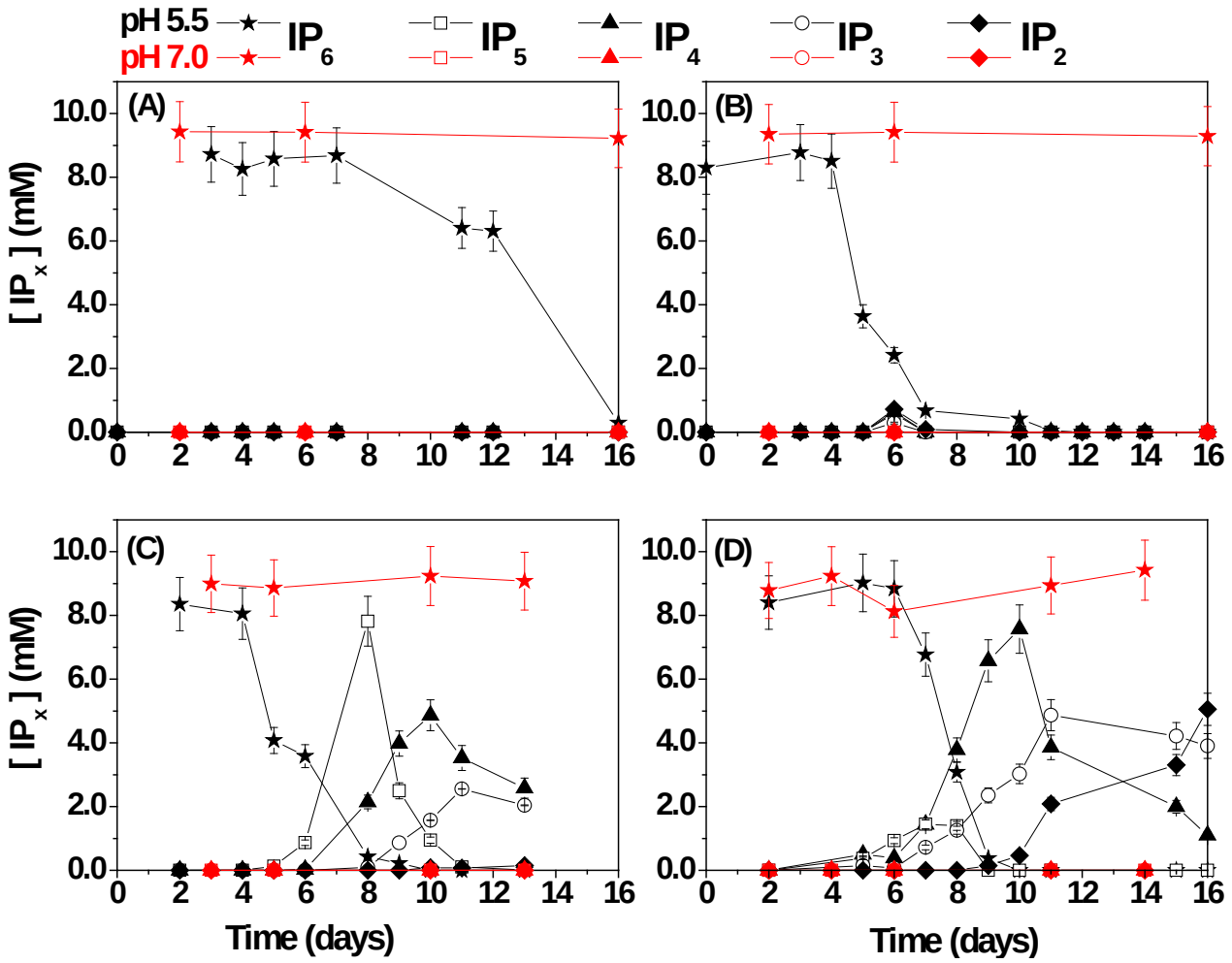

Figure 11. Evolution of inositol hexaphosphate (IP_6) and its lower derivatives (IP_x, x = 2:5) as a function of time in pH 5.5 (black) and pH 7.0 (red) slurries containing 16 g/L Area 3 Oak Ridge Field Research Center soils in artificial groundwater amended with A) 10 mM phytate (+ P - G - U); B) 10 mM phytate and 10 mM glycerol (+ P + G – U); C) 10 mM phytate, and 200 µM UO_2^{2+} (+ P – G + U); and D) 10 mM phytate, 10 mM glycerol, and 200 µM UO_2^{2+} (+P + G + U). Reactors buffered at pH 7.0 were also amended with 10 mM dissolved inorganic carbon. Error bars include variation between triplicate reactors and analytical error from calibrations.

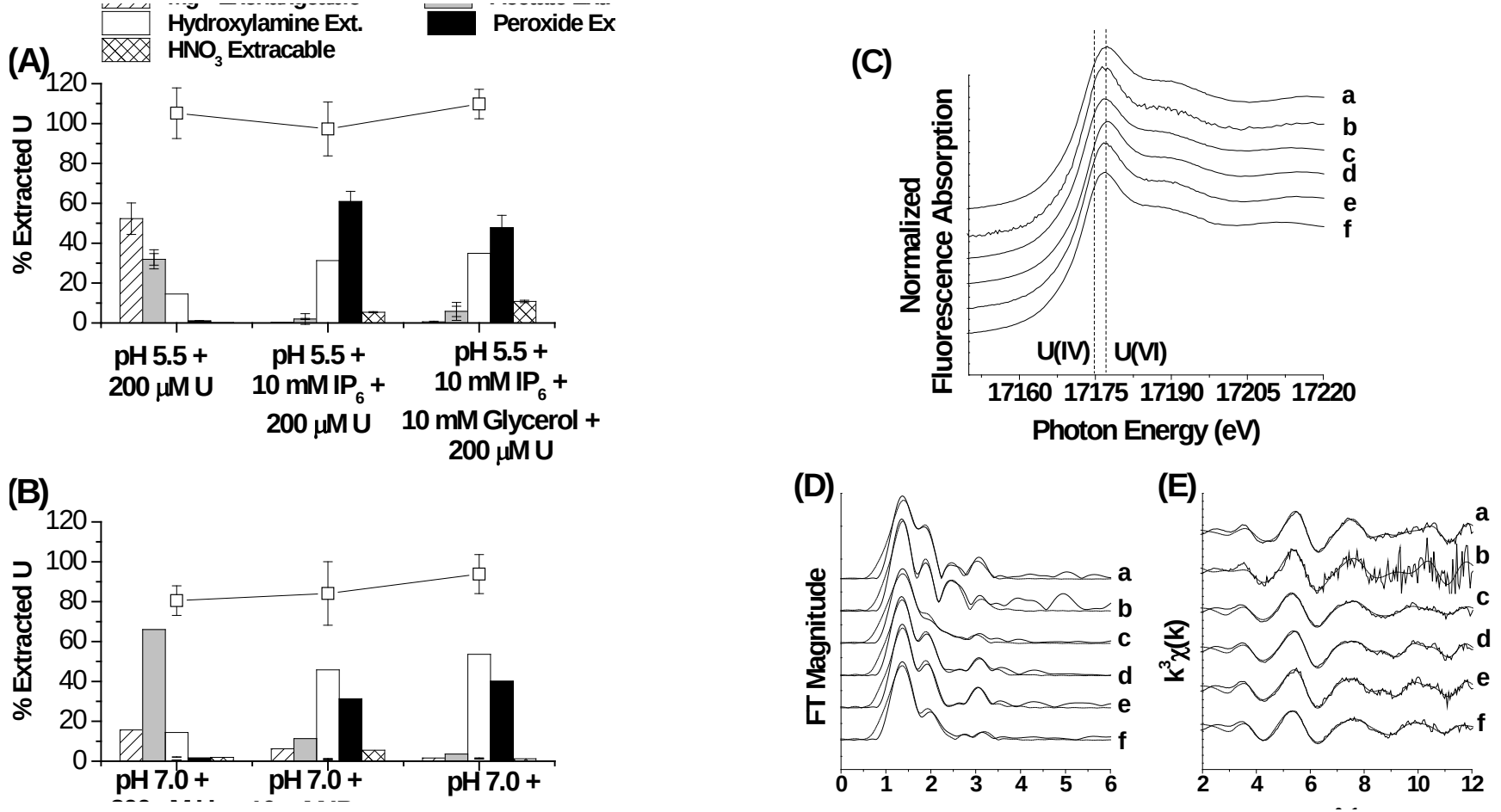

Figure 12. Solid phase-associated U extracted using a modified sequential extraction technique from pH 5.5 (A) and pH 7.0 (B) soil slurries of Area 3 of the Oak Ridge Field Research Center following aerobic incubation for 16 days. Bars represent the fraction of U extracted during each individual extraction step relative to total extracted uranium in each treatment. Symbols represent the percent uranium recovered in each treatment. All error bars include the variation between triplicate reactors and duplicate extractions. Uranium (C) XANES, (D) R-space, and (E) k-space diagrams of the L_{III}-edge EXAFS. Treatments included a: pH 5.5, 200 µM U; b: pH 5.5, 200 µM U + 10 mM IP_6; c: pH 5.5, 200 µM U + 10 mM IP_6 + 10 mM glycerol; d: pH 7.0, 200 µM U; e: pH 7.0, 200 µM U +10 mM IP_6; and f: pH 7.0, 200 µM U + 10 mM IP_6 + 10 mM glycerol.

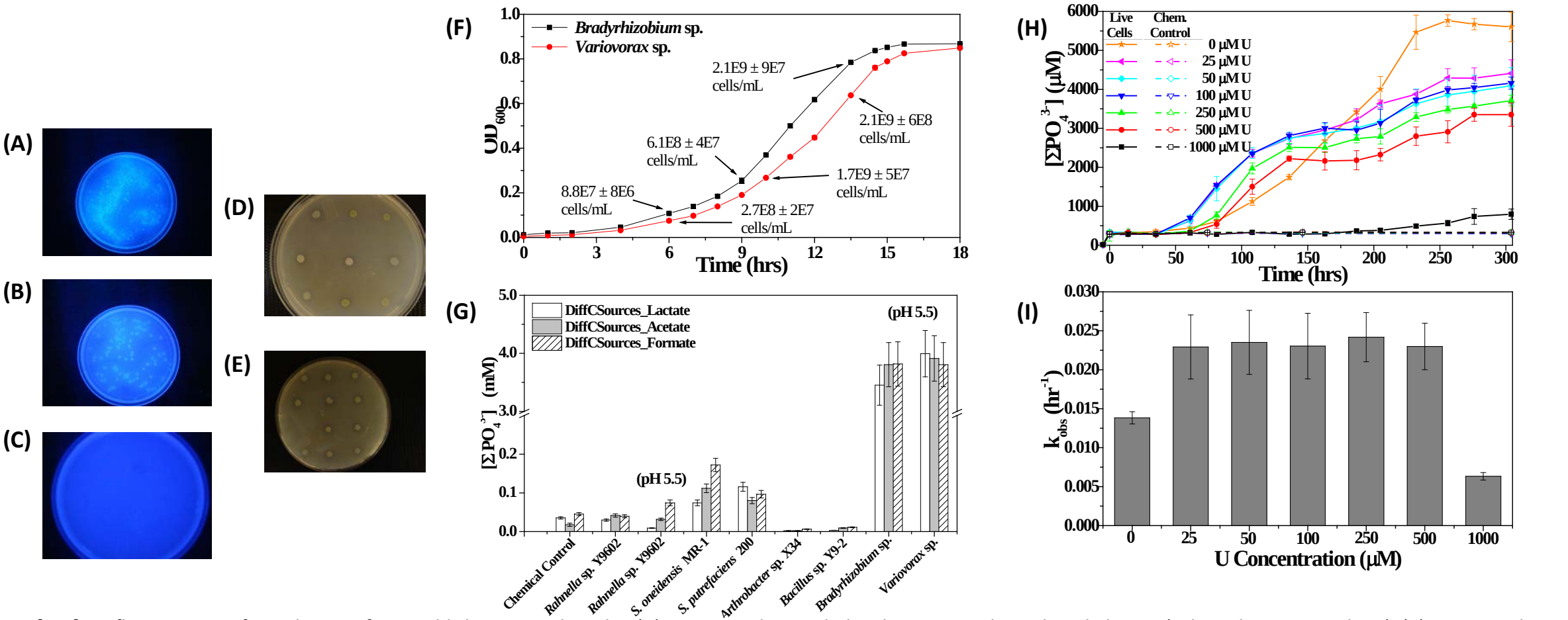

Figure 13. [A-C] UV fluorescence of enrichments from soild slurries incubated at (A) pH 7.0 and amended with uranium, glycerol, and phytate (sphingobacteria medium), (B) pH 5.5 and amended with uranium and phytate (1/10 nutrient broth medium), and (C) pH 7.0 and amended with uranium and glycerol, but no phytate (1% tryptone medium). Each soil slurry was serially diluted 10^4 times and grown at room temperature in the dark for 3 days onto agar plates containing enriched nutrient medium amended with 4-methylumbelliferyl phosphate (MUP), a compound which fluoresces upon hydrolysis of the phosphate group. [D-E]: Microbial isolates from (D) pH 7.0 and (E) pH 5.5 soil slurries amended with uranium and phytate plated onto enriched nutrient medium amended with phytate at pH 7.0 for 3 days in the dark. The clear halo around the colonies indicates expression of phytase activity. (F) Optical Density at 600 nm (OD_{600}) as a function of time of *Bradyrhizobium* sp. and *Variovorax* sp., two of the microorganisms isolated from the serial dilutions, incubated aerobically at pH 7.0 in nutrient broth media. Cell counts as determined by staining with acridine orange are provided at select time points. (G) Inorganic phosphate (ΣPO_4^{3-}) production after 1 week of incubation in aerobic cultures of *Rahnella* sp. Y9602, *Shewanella oneidensis* MR-1, *Shewanella putrefaciens* strain 200, *Arthrobacter* sp. X34, *Bacillus* sp. Y9-2, *Bradyrhizobium* sp., and *Variovorax* sp. relative to chemical controls. Incubations were conducted at pH 7.0 (unless otherwise noted) in artificial groundwater amended with 1 mM inositol hexaphosphate and 1 mM lactate, 1 mM acetate, or 1 mM formate as electron donors. (H) Production of ΣPO_4^{3-} as a function of time by *Variovorax* sp. initially exposed to increasing concentrations of UO_2^{2+} and incubated in aerobic conditions at pH 5.5 in artificial groundwater amended with 3 mM lactate and 1 mM phytate (solid symbols and plain lines) relative to chemical controls (open symbols and dashed lines). (I) Calculated pseudo-first-order rates constants (k_{obs}) for ΣPO_4^{3-} production by *Variovorax* sp. exposed to increasing uranium concentrations. Error bars of (F-H) represent the variation between triplicate incubations and the analytical error on duplicate measurements. Error bars of (I) represent the standard error of the slope of the linear regression used to calculate k_{obs}.

Figure 14. Positron emission tomography of sediment colums containing *Rahnella* sp. Y9602. (A) Schematic of soil column (left) and soil column in microPET scanner (right). (B) Two-dimensional PET projection of the soil column filled with fine sand and randomly seeded with activated carbon after exposure to 1.0 MBq mL−1 of ^{18}FDG for 1 h (27 Ci mL−1) followed by 6 h of deionized water, at a flow rate of 7.2 mL h−1. Each second represents a 10 min average of 511 KeV annihilation photons.

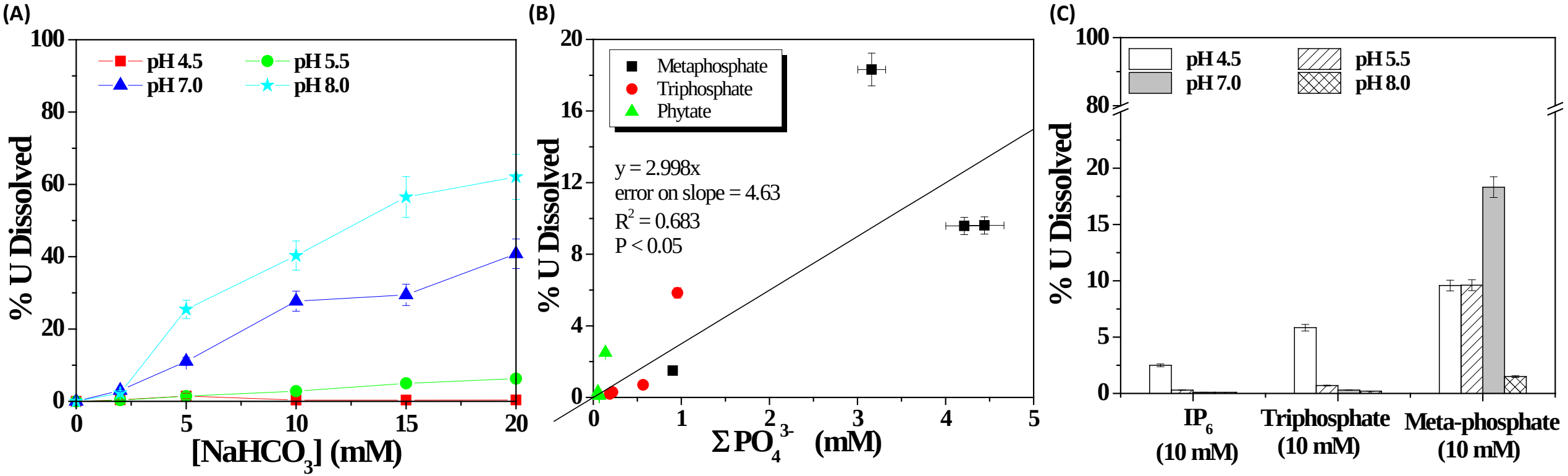

Figure 15. Percent dissolution of autunite equilibrated for 10 days in pH 4.5, 5.5, 7.0, and 8.0 artificial groundwater in the presence of (A) increasing carbonate concentrations; (B) increasing inorganic phosphate concentrations; and (C) 10 mM inositol hexaphosphate (IP_6), 10 mM triphosphate, or 10 mM meta-phosphate.
Error bars represent the variation between triplicate experiments and the analytical error on duplicate measurements